7.1 Introduction

Photo detectors lie in the class of electronic devices, mainly used to detect or sense the presence of photo (light), and have presented enormous potential applications in different field such as space communication, detection of missile-plume, monitoring of flame, etc.[Mueller et al. (2010), Sang et al. (2013), Omnès et al. (2007)]. A number of wide band gap organic as well as inorganic semiconductor materials, viz. ZnS, ZnO, GaN, SnO_2, graphene quantum dots, MoS_2 and its composite have been explored as active matrix for photoactive materials of photo detectors [Bilgaiyan et al. (2015), Sharma et al. (2010), Sharma et al. (2013), Singh et al. (2015), He et al. (1993)]. Among all, semiconducting, wide band gap materials, SnO_2 is a well-known n-type direct band gap (Eg~3.6 eV for bulk SnO_2) metal-oxide semiconductor, have already been interrogated as efficient parts in UV (visible-blind) photo detectors with high quantum efficiency in shorter wavelength region owing to its exceptional optical sensitivity [Semancik et al. (1990), Han et al. (2009), Kar et al. (2011), Li et al. (2015)]. Upto now, there are different nanostructures such as nanowires, nano rods, nano belts and nanotubes and thin films of inorganic materials which have extensively been studied and used as chemical/gas sensors for environmental and industrial electronic devices applications [Harrison et al. (1988), Leite et al. (2000), Zhang et al. (2014), Pandey et al. (2017), Hussain et al. (2014)]. Among all those, SnO_2 nanomaterial's, one-dimensional nanostructures, have attracted much attention due to high surface-to-volume ratio, are being considered as the building blocks for photo detectors having high performance with larger sensitivity, high quantum efficiency, and better response speed [Alvisi et al. (2001), Tatsuyama et al. (1976), Dazhi et al. (1994)]. It is noteworthy that the existence of deep-level surface trap states in one dimensional

nanostructures, are being caused by the enhanced surface to volume ratios which significantly extend the generation of photo carriers. Further, in low-dimensional devices, the active region's decreased dimensionality ultimately reduces the transit time of photo generated carrier. But for the anticipated outcome this is prime requirement to short out the particular synthesis route which handles the structure as well as morphology in easier way as it is found that there are several synthesis parameters over which the SnO_2 morphology is highly dependent. So there exist a number of synthesis routes, implemented for the preparation of SnO_2 nanostructures which comprises the solution evaporative decomposition method [Hu et al. (2002), Yeh et al. (1995)], sol-gel method [Han et al. (2005), Pang et al. (2001)], gas phase method [Liu et al. (2004), Ba et al. (2005)], wet chemical synthesis [Wang et al. (2003), Wang et al. (2008)] and laser ablation technique [Liu et al. (2003), Desarkar et al. (2012)]. Amongst all the synthesis routes listed above, hydrothermal route has got tremendous attention for synthesize of SnO_2 nanostructures for well-defined structures and due to its feasibility for the production of different nanostructures as per requirement via just changing synthesis parameter, simplicity, high efficiency, and low cost. On the other hand, the nanostructures morphologies and crystal structure can be regulated by varying some specific experimental parameter like time, temperature, pressure etc. [Talebian et al. (2013), Sōmiya et al. (2000)]. Short wavelength photo detectors constructed via one dimensional (1-D) SnO_2 nanostructures is not up to the mark and still show a poor photocurrent and inadequate stability, limit their further application in optoelectronics devices. Although, SnO_2 based one-dimensional nanostructures have high surface-to-volume ratio, having high performance with larger sensitivity, high quantum efficiency, and better response speed. But the poor photocurrent of SnO_2 which arises due to presence of large number of recombination sites, limit their

application. Therefore, the optoelectronic device formed by the hybridization of materials, have attracted much consideration due to enhancement in its greater optoelectronic properties, stability, and most importantly overcoming the several other limitations as compared to that of corresponding single materials. In this regards, graphene, one of the interesting two dimensional (2-D) materials and well testified for its exceptional physical properties such as high mechanical flexibility, transparency, as well as high electrical conductivity, can also exist in a single atomic layer in ambient condition due to its exceptional impermeability, has emerges as one of the promising materials for hybridization of SnO_2 nano wire [Luo et al. (2006), Chen et al. (2004), Hu et al. (2011)]. It is noteworthy that the Fermi level of graphene/rGO well fall between the conduction band and valence band of SnO_2 which cause charge transfer interaction between them. Therefore, the hybridization of graphene into the SnO_2 nanowires, a prominent photoactive material, can be assumed to offer the synergetic support in carrier transit during light absorption. Although, the graphene/inorganic semiconductors heterostructures still lacks the detailed study of junction in different configuration and wavelength dependent photocurrent yet presents studies related to hybridization, have shown the enhancement in its the photo detection performance.

In present work, we demonstrated the high performance photo detector based on SnO_2/rGO for short wavelength in optimized geometry Metal Semiconductor Metal (MSM) structure where exposer of whole active area occurred. Prior to fabrication of high performance photo detector, hydrothermal synthesis of SnO_2 nanowire, rGO via improved Hummer's method were carried out. Whereas, the hybridization of hydrothermally developed SnO_2 nanowire and developed reduced graphene oxide for high-performance, spectral selectivity, photo detectors was carried out using hydrothermal route at 120^0 C temperature for 24 h

and 50-55 Kg/cm^2 pressure. Further, as synthesised SnO$_2$, rGO, and SnO$_2$/rGO hybrid materials were characterized using HR-SEM, XRD, FT-IR, absorption spectra, and AFM image. Two strategies of photo detector have been employed for investigation of optoelectronics properties such as using Pt coated Si tip in AFM mode (across the film) (ITO/ SnO$_2$-rGO/ Pt) and field effect transistor mode (along the film) (Au/ SnO$_2$-rGO/Au) without gate voltage for investigation of photocurrent in ambient conditions at room temperature. The photo-response behaviour of a photo detector has been found to depend significantly on the structure of device, wavelength of light, as well as measurement condition etc. Optimized photo detector geometry based on Au/ SnO$_2$-rGO/Au shows a high photo response which is about two orders enhancement in photocurrent compared to dark current at shorter wavelength.

7.2. Experimental

7.2.1. Materials

Graphite flakes are purchased from Alfa Aesar (325 mesh), however sulfuric acid (H$_2$SO$_4$, 95–98%), phosphoric acid (H$_3$PO$_4$, 85%), potassium permanganate (KMnO$_4$, 99.9%), and hydrogen peroxide (H$_2$O$_2$, 50%) are purchased from Merck. Hydrogen chloride (HCl, 37%) was purchased from Sigma-Aldrich. Tin (IV) chloride pentahydrate (SnCl$_4$ 5H$_2$O, 98%) and absolute ethanol were purchased from Merck and Fisher Scientific respectively. Distilled water from Merck was used throughout the sample preparation. All chemicals were used as received without further purification.

7.2.2 Preparation of fibrous SnO$_2$/GO composite

(a) Synthesis of SnO$_2$ nanowires

The SnO$_2$ nanowires were synthesized via hydrothermal routes which have been reported somewhere else [Talebian et al. (2013), Guo et al. (2004), Vuong et al. (2011)]. Initially,

1.05g of $SnCl_4.5H_2O$ and 1.4 g of NaOH was dissolved in 40 ml de-ionized water under magnetic stirring condition (approx. 10 min) for formation of homogeneous solution. Further, a 40 ml absolute ethanol was added drop wise in solution slowly under magnetic stirring condition which finally gives the white precipitation after completion of this addition. The resultant mixture solution was further kept under stirring for 24 h before transferred into 150 ml Teflon-linked autoclave. The autoclave was placed in an oven under 190-210 ^0C reaction temperature for 24 hrs. After the completion of the reaction, the resulting solid product obtained, was filtered and washed severally by de-ionized water, absolute ethanol and finally dried at 120 ^0C in air for 24 h for further characterization and fabrication of hybrid materials.

(b) Synthesis of reduced Graphene Oxide (rGO)

GO was synthesized from the graphite flakes using Improved Hummers' method describe somewhere else [Abraham et al. (2014), Raghubanshi et al. (2017), Marcano et al. (2010)]. In this method, a mixture of concentrated H_2SO_4/H_3PO_4 (360:40 ml) was added to a mixture of graphite flakes (3.0 g) and $KMnO_4$ (18.0 g), which produce a slight exothermic to 30~40 °C. The whole reaction kept for stirring (12 h) with simultaneous heating at 50 ^0C. Further, the reaction was cooled to room temperature and poured onto ice (~400 mL) with 50% H_2O_2 (~2 mL). The filtrate was placed for centrifugation at 4000 rpm for 2h, and the supernatant was decanted away. The remaining solid material was washed in a series with 150 mL of water, 150 mL of 30% HCl, and 150 mL of ethanol (2 times), and the resulting suspension was filtered over a PTFE membrane with a 0.45 µm pore size. The solid obtained on the filter was vacuum-dried overnight at room temperature.   As

synthesized GO was further reduced using microwave reduction at 700W for 3 minutes burning forms rGO.

(c) Synthesis of SnO$_2$-rGO hybrid materials, deposition of film

Initially, a 1 mg/ml uniform dispersion of SnO$_2$ and rGO each was prepared in ethanol and mixed in 5:1 ratio. The as prepared mixture was placed into the Teflon liner autoclave (120 ^{0}C for 24 h) for synthesis of SnO$_2$/r-GO hybrid. After 24 h and successful completion of reaction, allow the autoclave to settle at room temperature to obtain the precipitate of SnO$_2$/rGO hybrid. Further, the precipitates remove and washed severally with distilled water to make it free from contaminations. The obtained powder was dried under vacuum to obtain SnO$_2$/rGO hybrid.

Prior to deposition of film, a 1 mg/ml SnO$_2$/r-GO hybrid was dispersed in ethanol for formation of uniform dispersion. The film was deposited on Glass, ITO, as well as SiO$_2$/Si substrate by spray method by placing, as obtained solution from autoclave, into nebulization chamber of baby's Nebulizer. In order to obtain complete dry and crystalline film, the film was annealed at 500 ^{0}C for 3 hours in a tube furnace under an atmosphere of nitrogen.

7.3 Results and Discussion

Surface Morphology:

Fig. 7.1(a-c) shows the SEM image of SnO$_2$ nanowire, r-GO and SnO$_2$/rGO hybrid material respectively at different magnification. The SEM image (Fig. 7.1 (a)) confirms the formation of the nanowire with bunch of very long undistorted nanowires. The diameter of wires were examined, and found to be of 18~20 nm.
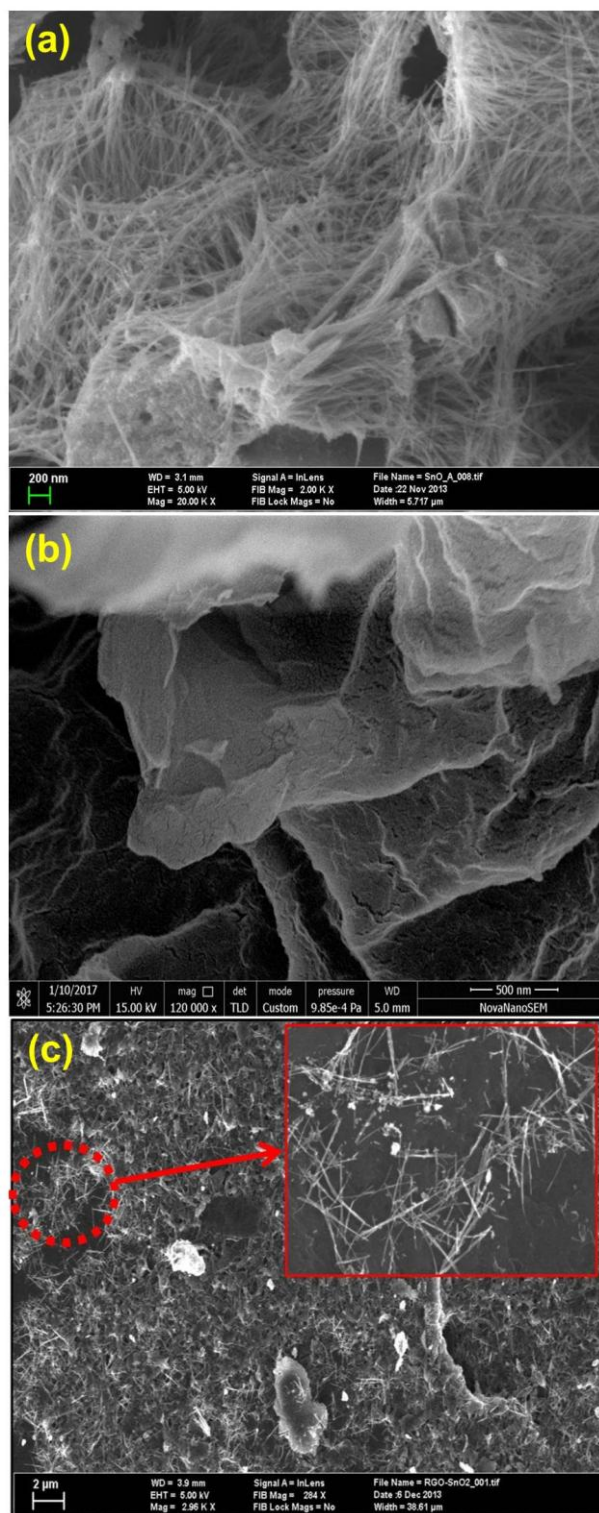
Fig. 7.1. SEM images of (a) synthesized SnO_2 nanowire, (b) rGO and (c) SnO_2/rGO film on SiO_2/Si substrate, Inset shows the zoom image of encircled region at 20KX magnification.

However, similar investigation was also conducted over rGO as shown in Fig. 7.1(c), which reveals the formation of flake structure; confirm the formation of rGO. Further investigation of SnO_2/rGO hybrid material film deposited over SiO_2/Si synthesized via hydrothermal route and deposited via medicine chamber of baby's spray nebulizer over SiO_2/Si, as shown in Fig. 7.1 (c), reveals the formation of SnO_2/rGO hybrid materials with well dispersed of rGO in SnO_2 nanowire matrix. Few nanowires are clearly visible over graphene (blackish layered) in SnO_2/rGO film hybrid film as shown in inset of Fig. 7.1(c).
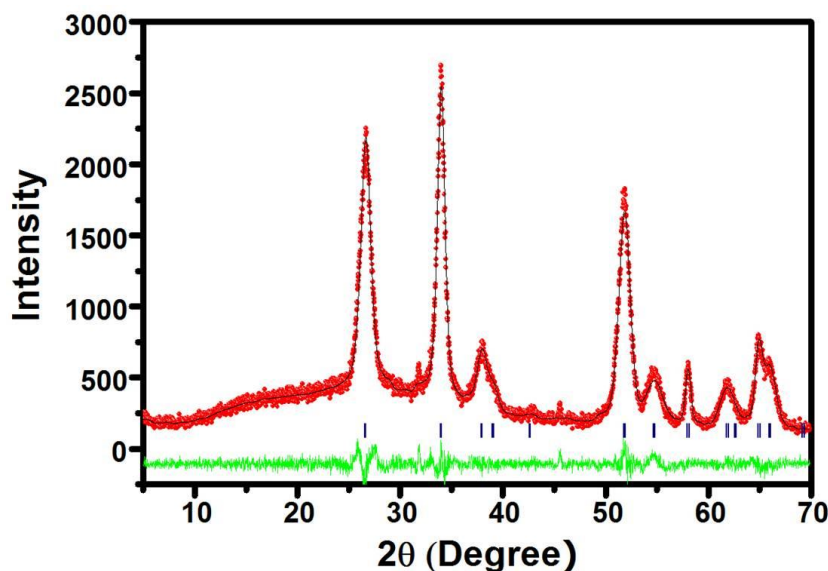
Structural Analysis:

Fig. 7.2. XRD of SnO_2 nano-wires. Observed (red dots), calculated (black line), and difference (green line), respectively.

In order to again confirm the formation of SnO_2 nano wire, XRD was conducted on as obtained hydrothermally grown nanostructures and, a Reitveld refinement studies was further employed on the as obtained XRD data (2Θ varying from the range of 5^0 to 70^0 with a step size of 0.02^0) using full prof suit as shown in Fig. 7.2. Here, observed (red dots), calculated (black line), and difference (green line) obtained after full pattern Reitveld

refinement in the 2Θ range 5^0-70^0 using P4$_2$/mnm structural model. In the refinement process, the background was initially modeled using six order polynomial and then by linear interpolation method, for peak shape we had used Pseudo-Voigt function which is a combination of the Gaussian and Lorentzian function. During the refinement, scale factor, FWHM parameters, lattice parameters, positional coordinates, zero displacement, thermal parameters were refined but occupancy parameters of the ions were kept constant at the nominal composition and has been shown in Table 7.1. Therefore, all the diffraction peaks can be readily indexed to the tetragonal phase of SnO_2 with calculated lattice parameters of a = 4.74A° and c = 3.17A° [Kar et al. (2011), Talebian et al. (2013)], which is looking similar to that of SnO_2 nanostructures. The tick marks above the difference (green line) show the position of Bragg peaks. Various refined parameter and agreement factors has been tabulated below

Table 7.1. Refinement parameters used in Reitveld and lattice parameter of SnO_2 obtained after Reitveld.

Ions	Positional coordinates			Thermal parameters
	X	Y	Z	$B(\mathring{A}^2)$
Sn^{3+}	0.000	0.0	0.000	0.1346
O^{2-}	0.29(3)	0.29(3)	0	0.01
a = 4.74(5), c = 3.17(9) (Å)				
$\alpha = 90.000 = \beta = \gamma$				
$\chi^2 = 2.34$				

The obtained data of XRD are also matched with JCPDS and well in agreement with the reported values (JCPDS card no. 77-0450). Further, the relatively higher intensity of diffraction peaks of nanowires demonstrates the higher crystallinity with the obtained

diffraction peaks, broadened by the small diameter of the nanowires. No impurity peaks are observed, indicating the high purity of the final products

Fig. 7.3 shows the XRD patterns of the as-synthesized SnO_2 nanostructures, as synthesized rGO, and rGO/SnO_2 hybrid. In the Fig. 7.3 (a) all the diffraction peaks can be readily indexed to the tetragonal phase of SnO_2 with calculated lattice parameters of a = 4.74A° and c = 3.17A° as discussed earlier [Han et al. (2009)]. Fig. 7.3(b) shows the XRD pattern of rGO with characteristics peak at 23 ^{0} which evident the formation of rGO However, Fig. 7.3(c) shows the XRD pattern of rGO/ SnO_2 hybrid which appear very similar to that of SnO_2 nanostructures as well as rGO. The peak intensity appears in pure SnO_2 nanostructure is reduced with formation of hybrid materials. The peak related to rGO is very weak and appear at same position as in pure rGO. This ruled out the formation of new phase during formation of hybrid materials.
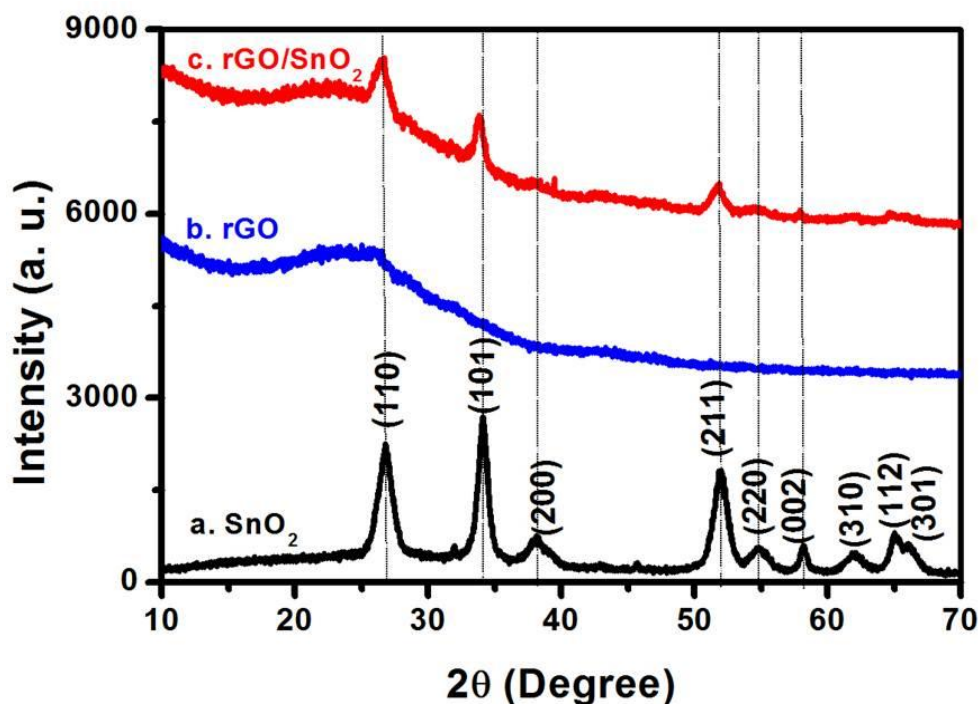

Fig. 7.3. XRD of (a) SnO_2 nanowire, (b) rGO and (c) SnO_2/rGO hybrid material.

Absorption Study:

The UV-Vis Transmittance spectra of SnO_2, rGO and SnO_2/rGO samples dispersed in ethanol and measured at room temperature as shown in Fig. 7.4. It is evident from Fig. 7.4(a) that SnO_2 nanowires absorb strongly at 218 nm whereas rGO shows strong absorption at 265 nm. The hybrid of SnO_2/rGO shows two absorption peak at 223nm and 268 nm, respectively. This phenomenon arises due to the presence of rGO with SnO_2 nanowire in solution which also led to increase the absorbance in visible region. Further, the transmittance spectra were also recorded for SnO_2/rGO hybrid materials, which exhibits very low transmittance for short wavelength and high transmittance in visible and near IR region as shown in Fig. 7.4(b). Thus, the obtained observation demonstrates the utility of this hybrid material in fabrication of short wavelength photo detector.
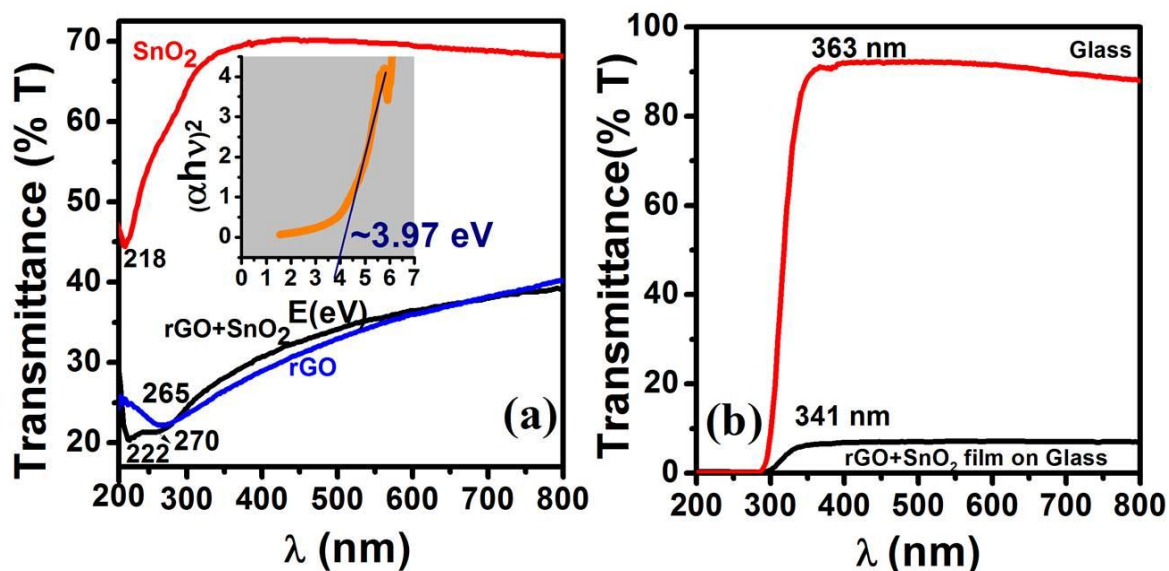

Fig. 7.4. UV-Vis Transmittance spectra of (a) SnO_2, rGO and SnO_2/rGo hybrid material in ethanol (Inset shows band gap energy plot for SnO_2) and (b) transmittance spectra of the glass as well as SnO_2/rGO deposited thin film on glass substrate.

The inset of Fig. 7.4(a) shows the band gap energy (E_g) plot for SnO_2 nanowires, indicating $E_g = 3.97$ eV, which is more as compared to that of bulk material (3.6eV). Same UV- Vis. Transmittance spectra has been obtained for the bare glass substrate as well as the rGO/SnO_2 thin film in the Fig. 7.4(b), which confirm the decrease in transparency of substrate after deposition.
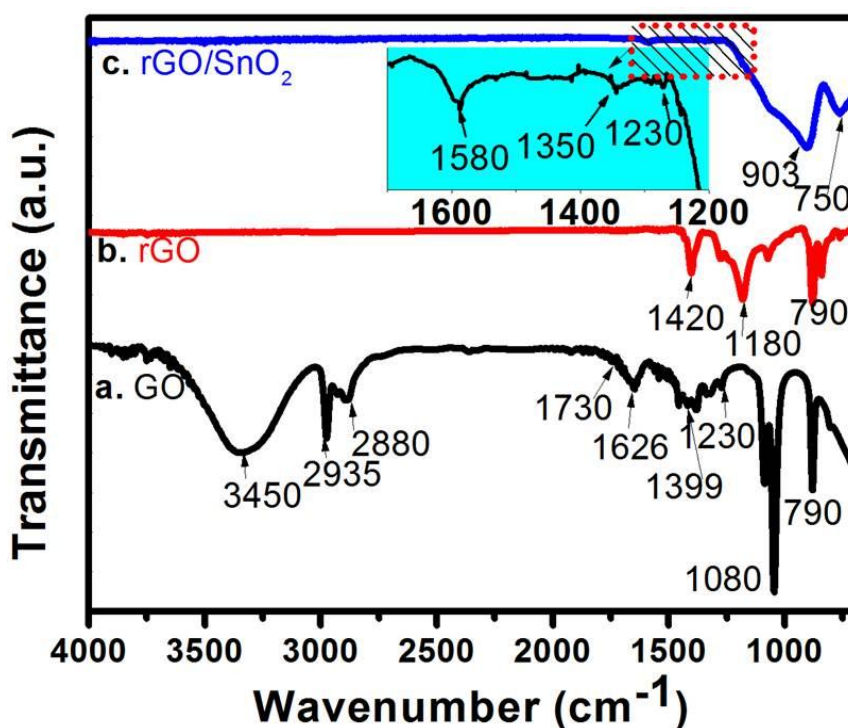
FT-IR study:

Fig. 7.5. The FTIR spectra of GO, rGO and SnO_2/rGO hybrid materials.

Fig. 7.5 shows the FTIR spectra of (a) GO, (b) rGO and (c) SnO_2/rGO hybrid materials, respectively. FT-IR spectrum of pure GO (Fig. 7.5 (a)) shows the peaks at 3450 (broad peak) and 1399 cm^{-1} which are assigned to O-H stretching and deformation vibrations, respectively whereas presence of two intense absorption band doublet at 2935 cm^{-1} and 2880 cm^{-1}, corresponds to symmetric and anti-symmetric stretching vibrations of –CH$_2$ group, respectively. [Bose et al. (2012)]. Furthermore, the appeared peaks around 1730,

1626, 1230, 1080, and 790 cm^{-1} , respectively confirm the presence of C=O stretching vibrations from carbonyl groups, C=C vibrations from the aromatic carbon, C-OH stretching vibrations, C-O vibrations from epoxy groups, and C-O vibrations from alkoxy groups in GO [Uddin et al. (2015), Bose et al. (2010), Kumar et al. (2014)]. The FT-IR spectrum of rGO (Fig. 7.5. B) does not encompass a peak for the epoxide group. However, low intensity hydroxyl group peaks are appear at 1180 cm^{-1} as compare to GO [Bose et al. (2012)]. Thus, the restoration of C=C stretching (at 1420 cm^{-1}) and the removal of peaks related to the oxygen functional groups in the particular spectrum of rGO confirms the successful reduction of GO during the microwave reduction. Further several time investigation of spectrum of hybrid materials (rGO-SnO$_2$) synthesized via hydrothermal method as discussed in experimental section (as shown in Fig. 7.5(c)) reveals the presence of C= C (moderate bonding at 1600 cm^{-1}), C=C (strong bonding at 750 cm^{-1}), C-OH (at 1350 cm^{-1}), C-O-C (at 1230 cm^{-1}) and one additional peak of O-Sn-O (at 903 cm^{-1}). It is important to note that the energy levels of r-GO fall within the band gap of SnO$_2$ which may cause the charge transfer (CT) interaction between them. The r-GO has shown better chemical stability but still having some defect over its nano sheets. In spite of this chemical stability of (as reported in literature) of rGO, the synthesis of hybrid materials carried out at 120^0 C for 24 hr. at 50-55 kg/cm^2 pressure. Thus, hydrothermal route causes the production of defect over rGO sheet and SnO$_2$ nanowire which further causes the CT interaction between rGO nanosheets and SnO$_2$ nanowire Therefore, the shifting of C=C from 1420 cm^{-1} to 1600 cm^{-1} arises due to interaction between defects over r-GO (C=C) and presence of defect over SnO$_2$ nanowire. Therefore, it is quite obvious from the FT-IR spectrum of hybrid materials that r-GO as well as SnO$_2$ are uniformly present with interaction between them via C=C and either defects or unsaturated bond over SnO$_2$ nanowire which again

support the SEM morphology, XRD and absorption spectra. It is also observed in hybrid materials spectrum that –OH bonding (usually present at ~3550 cm^{-1}) is absent which confirm the further reduction of rGO during hydrothermal chemical synthesis. Thus, appearance of some new peak with shifting of old peak of rGO confirms the existence of weak interaction among rGO nano-sheet and SnO_2 nanowire.

AFM Study:

The as-synthesized hybrid materials was deposited over solid substrate via spray method as discussed in experimental section and characterized using AFM. Fig. 7.6 shows the AFM topography with scanning area of size 90μm-90μm of SnO_2/r-GO hybrid materials deposited over SiO_2 (inset shows the height profile of the film). The estimation of average roughness (R_a) and root mean square roughness (R_q) of the film was found to be of 198 nm and 240 nm, respectively.
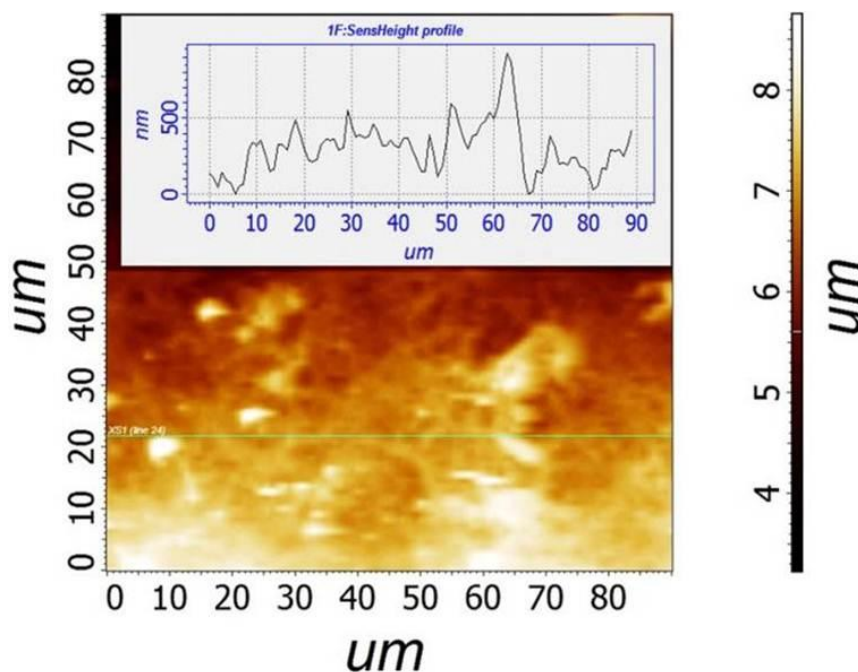

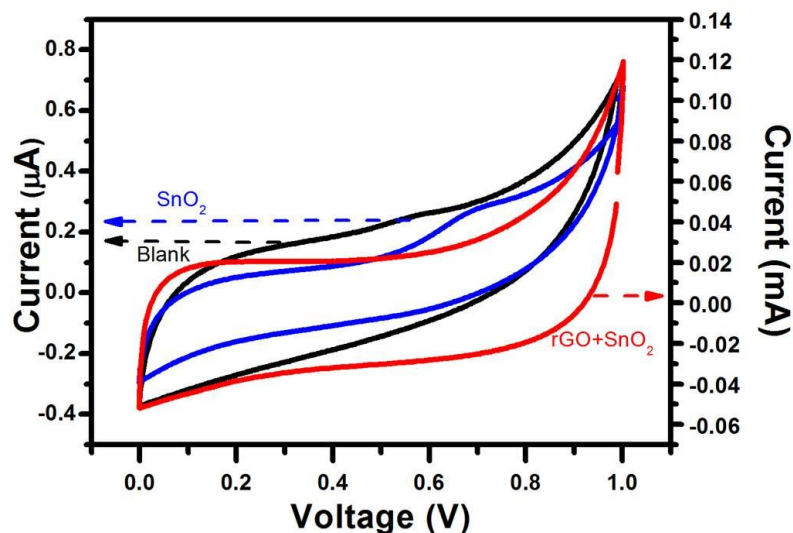**Fig. 7.6.** AFM topography of SnO_2/r-GO hybrid film deposited over SiO_2.

Cyclic Voltammetry Study:

Fig. 7.7. CV of bare glassy electrode, SnO_2 and SnO_2/r-GO respectively

Prior to investigation of optoelectronic property, the qualitative investigation of conductivity and electrochemical property of material was carried out using CV. Therefore, CV was used with three electrode cell assemblies having Ag/AgCl, as reference electrode while SnO_2 and SnO_2/r-GO, as hybrid coated glassy carbon as working electrode. A 0.1 M tetrabutyl ammonium perchlorate (TBAP) in acetonitrile solution with 50 mV scanning rate in range from 0.0 to 1 V vs Ag/AgCl were used for CV measurements using an electrochemical workstation. Thus, the electrochemical as well as conducting property (qualitative) of SnO_2/r-GO was investigated via CV and compared with SnO_2 at scan rate 50mV/s as shown in Fig. 7.7. Due to very high band gap, CV of SnO_2 shows very less current (less conducting). However, the CV of SnO_2/rGO hybrid shows the enhancement in current as compare to pure SnO_2 which can be justified via synergic support between rGO and SnO_2 where synergic support provided by conducting filler rGO. [Kim et al.

(2015)]. Meanwhile, rGO provide path to facilitate the charge transport through SnO_2 and resulting significant high current as compare to pure SnO_2 nanowire (more conducting).

Fabrication of device and study of Photo detection properties:

After the fabrication of thin film (as discussed in sec. 7.2c), MSM structure were fabricated by thermal vacuum evaporation in vacuum ($\sim 3*10^{-6}$ mbar) (model: HIND HIVAC model 12A4D) using metal shadow mask by depositing Au respectively. The thickness of metal electrode film was pre-adjusted to 80 nm in both case by digital monitor unit attached with quartz crystal microbalance.

The photo detection property of SnO_2/rGO film have been investigated via two ways (i) across the film via using Pt coated Si conducting tip in AFM mode, and (ii) along the film using transistor mode.
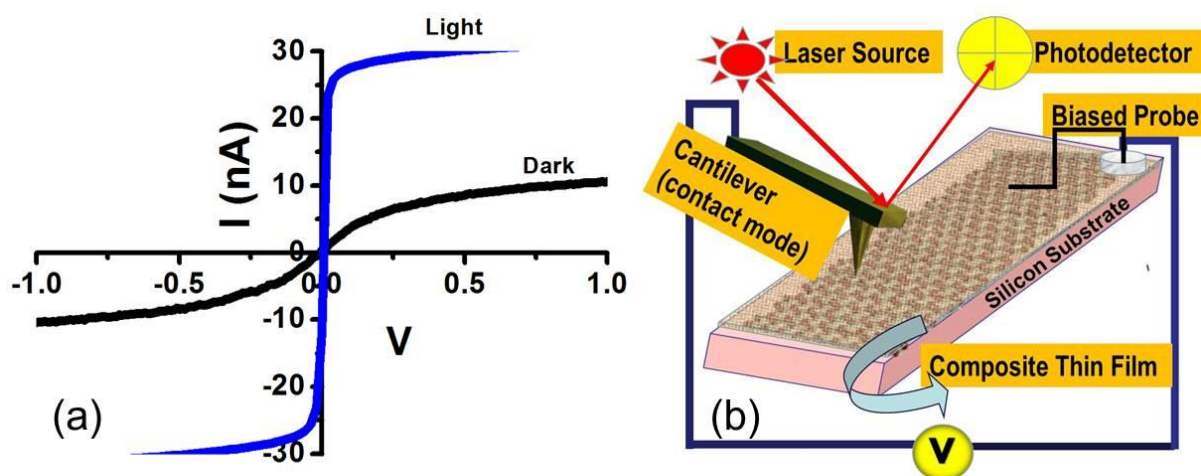

Fig. 7.8. (a) I-V characteristics of the thin film (ITO on Glass substrate) taken by Pt coated conducting Si tip in AFM mode, schematically represented in (b).

The I-V characteristic for the same film was measured in AFM using Pt coated Si conducting tip by applying the 5V bias voltage in contact mode under dark and bright illumination with the laser of 650 nm wavelength as shown in Fig. 7.8. Fig. 7.8(b) shows

the schematics of I-V measurements using conducting AFM tip in dark and illuminated condition where Pt coated Si tip was used as one electrode and biased probe used as second electrode. Finally I-V characteristic was recorded between ±1 V under dark and illumination as shown in Fig. 7.8(a). The obtained I-V curve under dark condition demonstrate the changes in the tip current by variation in the applied voltage under dark condition, however, illumination of junction with laser light cause enhancement in current by three fold from 10 nA to 30 nA. The enhancement in current occurs due to generation of photoelectron after illumination of junction which causes the enhancement in current. The mechanism of generation of photocurrent has discussed in later section.
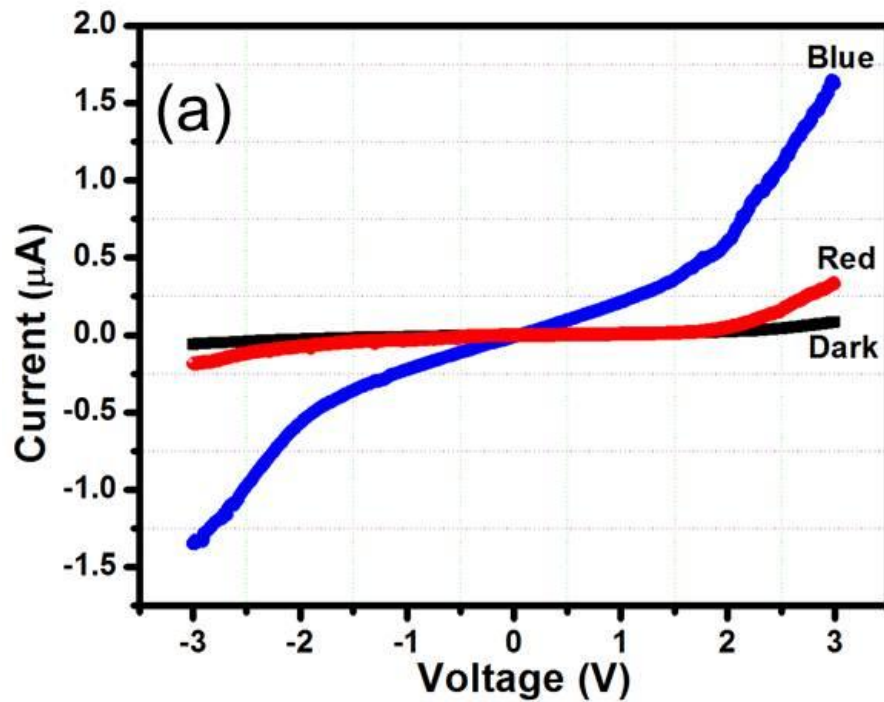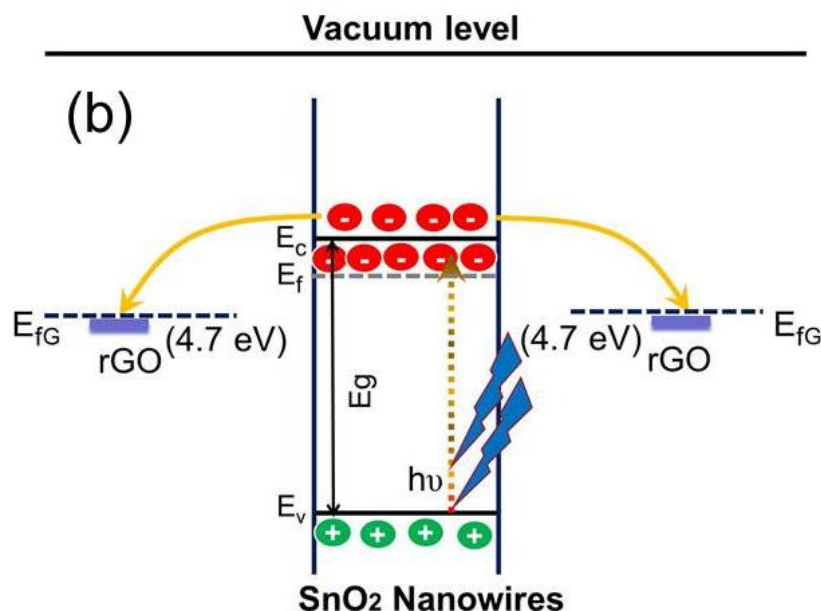
Fig. 7.9. (a) I-V characteristics SnO_2/rGO hybrid material in Au-SiO_2/ rGO-Au structure along the film under FET configuration without gate voltage under dark condition and illumination of red and blue light, respectively. (b) Schematics of generation of photo current after illumination.

Further the same film (rGO/SnO_2) deposited on SiO_2/Si substrate (p- type) as discussed in experimental section and photo detection property was investigated via MSM structure where film was fully exposed to blue light and red light as shown in Fig. 7.9(a). It is quite obvious from results that the obtained current is very low in dark condition and illumination causes the enhancement in current which confirm the generation of photoelectron in presence of either red light or blue light. Meanwhile, comparison of photocurrent with dark current reveals the much better enhancement by about 2 orders after illumination of blue light as compare to red one. The enhancement in current can be explained and understand on the schematic diagram as shown in Fig. 7.9 (b). It depicts the schematic diagram for charge-transfer among SnO_2/rGO photodetector under dark as well as light illuminations, respectively. It has already been reported in literature that SnO_2

nanowire is very sensitive for sorter wavelength due to high band gap, improved surface area which significantly prolong the generation of photo carriers and illumination of SnO_2 nanowire present in active region cause absorption of light and subsequently generation of electron-hole pairs in photoactive SnO_2 nanowire [Alvisi et al. (2001), Tatsuyama et al. (1976)]. Meanwhile, SnO_2 have higher level of conduction band as compare to the Fermi level of rGO which fall well between the bandgap of SnO_2 as shown in Fig. 7.9(b). Therefore, there exist a CT interaction between SnO_2 nanowire and rGO. The illumination of active region having SnO_2 nanowire with sorter wavelength cause generation of photo electron in conduction band which continuously undergo to highly conducting rGO channels via a charge-transfer process as shown in Fig. 7.9(b). It is quite obvious from Fig. 7.9(b) that there is no barrier during charge transfer process from SnO_2 to rGO. Thus, the recombination process of electron-hole pair during transit was reduced drastically due to high charge-carrier mobility of rGO which enhance the photocurrent of our device that makes our MSM structured photo-devices with high performances at a low bias in ambient conditions. The obtained result is higher as compare to other semiconductor nanowire-based photo detectors as reported in previous study [Li et al. (2015), Harrison et al. (1988)], which again confirm the effective utilization of the present thin SnO_2 nanowires with very high surface-to-volume ratio as the building blocks of UV photodetectors.

In summary, the hybridization of SnO_2 nanowire with conducting/Semiconducting rGO roots the amendment of photodetection and photocurrent. The morphological study of SnO_2 and SnO_2/rGO hybrid via SEM validate the formation of nanowire and uniformly distributed hybrid film. The obtained information was again validated via XRD, absorption spectra, FTIR. Accordingly, the hybridization roots the enhancement in photocurrent and detection property. Therefore, this manuscript has fruitfully validated the requirement of

hybridization prior to construction of photo detector thus flagging a way towards enhancement in photocurrent for high performance short wavelength photo detector.

7.4. Conclusion

We presented a facile and efficient method for the hybridization of SnO_2 nano wire with rGO nano sheet and fabrication of MSM structure for enhancement in photocurrent. Prior to synthesis of hybrid, SnO_2 nanowire synthesized via hydrothermal chemical route. However, rGO was synthesizes via improved Hummers method with successive microwave reduction. The hybrid film of SnO2/rGO was deposited over the solid substrates via spray method by placing the hybridized materials suspension inside the medicine chamber of baby's spray nebulizer. The structural property of SnO_2, rGO, SnO_2/rGO examined via XRD and retvield refinement which reveals formation of the SnO_2 nanowire, and hybrid of SnO_2/rGO. Further, spectral properties investigation is carried out via UV-Vis spectroscopy and FTIR analysis, and whereas morphological investigation via SEM. AFM confirms the nanowire formation and formation of nano hybrid material. The I-V characteristics of film was conducted via metal- semiconductor- metal (MSM) structure, sandwiched structure using STM tip in dark and in presence of light using different wavelength light source and found wavelength dependent photo detector with drastic enhancement in photocurrent (10^2 order) at ± 3 V for shorter wavelength. Thus, our material is selective for light source and can be used further for selective photo detector.